

1-27-2012

# A Nano-Cheese-Cutter to Directly Measure Interfacial Adhesion of Freestanding Nano-Fibers

Xin Wang

Johnny F. Najem  
*University of Akron Main Campus*

Shing Chung Josh Wong  
*University of Akron Main Campus, swong@uakron.edu*

Kai-tak Wan

Please take a moment to share how this work helps you [through this survey](#). Your feedback will be important as we plan further development of our repository.

Follow this and additional works at: [http://ideaexchange.uakron.edu/mechanical\\_ideas](http://ideaexchange.uakron.edu/mechanical_ideas)



Part of the [Mechanical Engineering Commons](#)

---

## Recommended Citation

Wang, Xin; Najem, Johnny F.; Wong, Shing Chung Josh; and Wan, Kai-tak, "A Nano-Cheese-Cutter to Directly Measure Interfacial Adhesion of Freestanding Nano-Fibers" (2012). *Mechanical Engineering Faculty Research*. 342. [http://ideaexchange.uakron.edu/mechanical\\_ideas/342](http://ideaexchange.uakron.edu/mechanical_ideas/342)

This Article is brought to you for free and open access by Mechanical Engineering Department at IdeaExchange@UAKron, the institutional repository of The University of Akron in Akron, Ohio, USA. It has been accepted for inclusion in Mechanical Engineering Faculty Research by an authorized administrator of IdeaExchange@UAKron. For more information, please contact [mjon@uakron.edu](mailto:mjon@uakron.edu), [uapress@uakron.edu](mailto:uapress@uakron.edu).

**A nano-cheese-cutter to directly measure interfacial adhesion of freestanding nanofibers**

Xin Wang, Johnny F. Najem, Shing-Chung Wong, and Kai-tak Wan

Citation: [Journal of Applied Physics](#) **111**, 024315 (2012); doi: 10.1063/1.3677947

View online: <http://dx.doi.org/10.1063/1.3677947>

View Table of Contents: <http://scitation.aip.org/content/aip/journal/jap/111/2?ver=pdfcov>

Published by the [AIP Publishing](#)

---

**Articles you may be interested in**

[Fabrication and characterization of silver- and copper-coated Nylon 6 forcespun nanofibers by thermal evaporation](#)

[J. Vac. Sci. Technol. A](#) **32**, 061401 (2014); 10.1116/1.4896752

[A comparative study of spin coated and floating film transfer method coated poly \(3-hexylthiophene\)/poly \(3-hexylthiophene\)-nanofibers based field effect transistors](#)

[J. Appl. Phys.](#) **116**, 094306 (2014); 10.1063/1.4894458

[Microwave absorption properties of helical carbon nanofibers-coated carbon fibers](#)

[AIP Advances](#) **3**, 082112 (2013); 10.1063/1.4818495

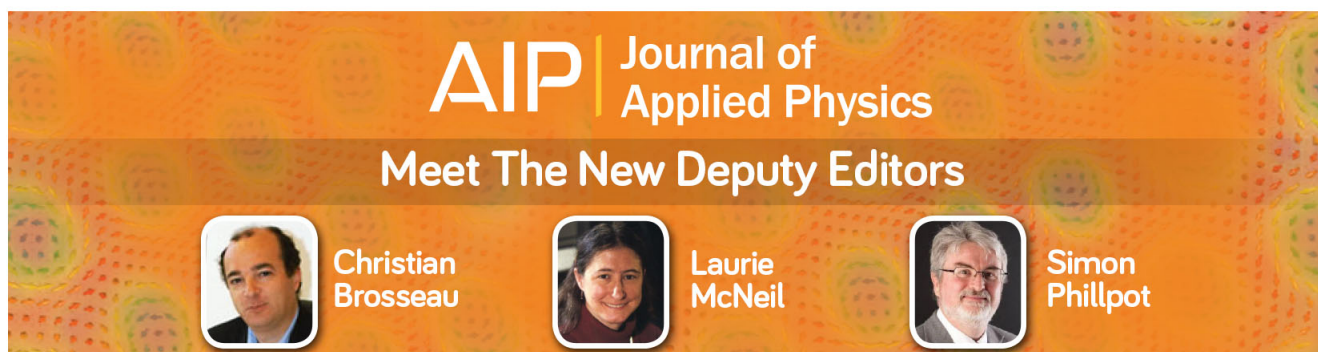
[Direct measurement of bending stiffness and estimation of Young's modulus of vertically aligned carbon nanofibers](#)

[J. Appl. Phys.](#) **113**, 194308 (2013); 10.1063/1.4803853

[3D mechanical measurements with an atomic force microscope on 1D structures](#)



[Rev. Sci. Instrum.](#) **83**, 023704 (2012); 10.1063/1.3681784

---



**AIP** | Journal of Applied Physics

**Meet The New Deputy Editors**

	<b>Christian Brosseau</b>		<b>Laurie McNeil</b>		<b>Simon Phillpot</b>
---	---------------------------	---	----------------------	---	-----------------------

# A nano-cheese-cutter to directly measure interfacial adhesion of freestanding nano-fibers

Xin Wang,<sup>1</sup> Johnny F. Najem,<sup>2</sup> Shing-Chung Wong,<sup>2</sup> and Kai-tak Wan<sup>1,a)</sup>

<sup>1</sup>Mechanical & Industrial Engineering, Northeastern University, Boston, Massachusetts 02115, USA

<sup>2</sup>Mechanical Engineering, University of Akron, Akron, Ohio 44325, USA

(Received 21 October 2011; accepted 14 December 2011; published online 27 January 2012)

A nano-cheese-cutter is fabricated to directly measure the adhesion between two freestanding nano-fibers. A single electrospun fiber is attached to the free end of an atomic force microscope cantilever, while a similar fiber is similarly prepared on a mica substrate in an orthogonal direction. External load is applied to deform the two fibers into complementary V-shapes, and the force measurement allows the elastic modulus to be determined. At a critical tensile load, “pull-off” occurs when the adhering fibers spontaneously detach from each other, yielding the interfacial adhesion energy. Loading-unloading cycles are performed to investigate repeated adhesion-detachment and surface degradation. © 2012 American Institute of Physics. [doi:10.1063/1.3677947]

## I. INTRODUCTION

Freestanding structures are ubiquitous in the modern era of nanotechnology, especially in electronics, nano-materials development, bioengineering, and nano-fiber meshes. In micro- and nano-electromechanical systems (M/NEMS), beams, bridges, diaphragms, and switches are indispensable components. Performance and reliability of the micro-devices depends critically on the adhesion or stiction of these freestanding components in the presence of intersurface forces, electrical field, and environment such as moisture and meniscus.<sup>1,2</sup> Nano-fibers produced by electrospinning<sup>3,4</sup> are used in protective clothing,<sup>5</sup> orthopedic prosthesis,<sup>6</sup> biomedical scaffolds,<sup>7</sup> and drug delivery.<sup>8</sup> Extensive theoretical modeling and experimental techniques are developed in the literature to characterize nano-structures such as graphene,<sup>9</sup> nano-fibers,<sup>10</sup> carbon nano-tubes,<sup>11,12</sup> gecko's satae,<sup>13</sup> and DNA chain,<sup>14</sup> but direct measurement of fiber-fiber adhesion to a high resolution is unavailable in the literature. The need for a viable method is even more pronounced in characterizing the mechanical integrity of a fiber mesh in terms of the stiffness and adhesion of individual fibers.<sup>15,16</sup> The indispensable interfacial properties of fiber-fiber adhesion is by and large ignored in the literature, though it is obvious that without which the mesh cannot stay intact mechanically upon external loads.<sup>17</sup>

In this paper, we report a novel *nano-cheese-cutter* to characterize freestanding nano-fibers for their elastic modulus and inter-fiber adhesion with nN and nm resolutions. The method can be readily adapted for other aforementioned 1-dimensional structures. The celebrated surface force apparatus<sup>18</sup> measures the intersurface forces between two atomically smooth surfaces in a crossed-cylinder configuration. Here we adopt a similar geometry for freestanding fibers, and will experimentally investigate behavior of electrospun fibers as a demonstration. A theoretical model will be derived from the first principles to extract materials parameters from experiments.

<sup>a)</sup>Author to whom correspondence should be addressed. Electronic address: ktwan@coe.neu.edu.

## II. EXPERIMENT

Sample preparation, experimental setup, adhesion measurements, and data analysis are discussed in details. Lengthy derivation of the theoretical model is given in Appendixes A and B.

### A. Sample preparation

Electrospun nano-fibers were fabricated as follows. Nylon 6 pellets (Sigma Aldrich CAS 25038-54-4) with density  $1.084 \text{ g} \cdot \text{ml}^{-1}$  were dissolved in 88% formic acid (EMD Corporation CAS 64-18-6). The solution was diluted to 25% in weight and magnetically stirred overnight. A syringe pump generated a pressure to maintain a sessile drop at the tip of a 0.559 mm gauge 21 stainless steel needle. The 25 mm long needle was attached to a 5 ml syringe filled with the aforementioned solution. Electrospinning was then performed with solution feed rate ( $FR$ ) at  $2.0 \mu\text{l} \cdot \text{min}^{-1}$  and applied voltage at  $V = 20 \text{ kV}$  at ambient temperature and relative humidity of 50%. The nano-fibers produced were collected by a  $\phi 150 \text{ mm}$  rotational disk collector at a take-up velocity ( $TUV$ ) of  $14.2 \text{ m} \cdot \text{s}^{-1}$ . Nano-fibers of desirable diameter range and crystal alignment can be adjusted by varying  $FR$ ,  $V$  and  $TUV$  simultaneously or separately.

### B. Fixture for nano-cheese-cutter

A flat tipless atomic force microscope (AFM) cantilever (Applied NanoStructure, Inc.) was chosen to support the sample fiber because of its high precision in force and displacement measurement. The deflection sensitivity was calibrated by repeated contact mode indentation on a freshly cleaved muscovite mica surface in air with sweep duration of 1.04 s, and the spring constant was found to be  $0.152 \pm 0.02 \text{ N} \cdot \text{m}^{-1}$  by the Cleveland method.<sup>19</sup> Using a high resolution micro-manipulator (AutoMate Scientific) combined with a stereomicroscope (Olympus, BX51), two identical glass microspheres with a diameter of 30–50  $\mu\text{m}$  (Potters Industries) were attached to the free end of an AFM cantilever using epoxy (AeroMarine TM 400) with a

designated separation of 50–120  $\mu\text{m}$  (Fig. 1(a)). The epoxy was then cured after 2 h at 90°C. A complementary pair of microspheres was similarly attached to the surface of an atomically smooth mica sheet (Fig. 1(b)). Before any fibers were attached to the spheres, the baseline of zero applied load,  $F=0$ , was established. Using an inverted optical microscope (Olympus, GX 71), the cantilever was precisely positioned such that the midpoint of the sphere-sphere separation on AFM cantilever was immediately above that of the other two spheres on mica in an orthogonal orientation. An AFM (Agilent 5500) then measured forces as the cantilever being slowly driven vertically downwards through a displacement of  $w_0$  while  $F(w_0)$  was recorded simultaneously. The intersurface forces between the spheres and mica surface were measured consistently and repeatedly in nano-Newton range. All force measurements hereafter had such baseline taken into considerations.

### C. Nano-cheese-cutter

A freestanding electrospun fiber was picked up by micro-capillary needles (Tritech Research) using the micro-manipulator. Both ends of a taut fiber were glued by epoxy to the two microspheres on AFM cantilever, forming a *nano-cheese-cutter*, now aligned with the cantilever axis (denoted by subscript 1 hereafter) as shown in Fig. 1(a). Another similar fiber was similarly attached onto the microspheres on mica (denoted by subscript 2) as shown in Fig. 1(b). The fiber diameter,  $d_i$ , and the fiber length,  $2l_i$ , were freely chosen, and were measured post-mortem by scanning electron microscopy (SEM, Carl Zeiss AG Supra 25). The fibers were made as taut as possible, but sagging remained inevitable which will show up in subsequent measurements (see later section). Orthogonal crossed-cylinder geometry was adopted

here. The cheese-cutter was then driven vertically downwards to interact with the other fiber (Figs. 1(c) and 1(d)). Both quasi-static and loading-unloading cycles were performed. Throughout the loading process, the rigid epoxy did not show any yielding or slippage at the fiber-microsphere, cantilever-microsphere, and mica-microsphere junctions.

### D. Mechanical characterization and adhesion measurement

Figure 2 shows loading (ABC) and unloading (CDGHJK) trajectories. Along AB, the fibers were either too far apart to be interacting or one sagging fiber simply hung on the other fiber with its negligible weight. No long range intersurface force was measured along AB. At B, the fibers were in adhesion contact and both became taut. Further compression along BC stretched the cheese-cutter into an inverted V-shape and the lower fiber into a complementary V-shape. The theoretical constitutive relation is given in Appendix A. Since  $(w_0/d) > 3$ , the fiber appears thin and flexible, and elastic stretching is the dominant deformation mode. The constitutive relation of a single fiber is given by equation (A9) to be  $F = (\pi E d^2 / 4 l^3) w_0^3$ . For two interacting fibers, the vertical forces acting on each fiber are of the same magnitude ( $F_1 = -F_2$ ), therefore,

$$F = \frac{\pi E}{4} \left( \frac{l_1}{d_1^{2/3}} + \frac{l_2}{d_2^{2/3}} \right)^{-3} w_0^3, \quad (1)$$

where  $w_0 = (w_0)_1 + (w_0)_2$  is now the total central displacement of the two fibers. The relation  $F \propto w_0^3$  yields a linear dependence of  $\log[F/(\pi d^2/4)]$  upon  $\log[(w_0)_2/l_2]$  with slope of 3. Figure 2(b) shows the force data along BC in a log-log plot against the expected cubic relation of  $F(w_0)$ . The elastic

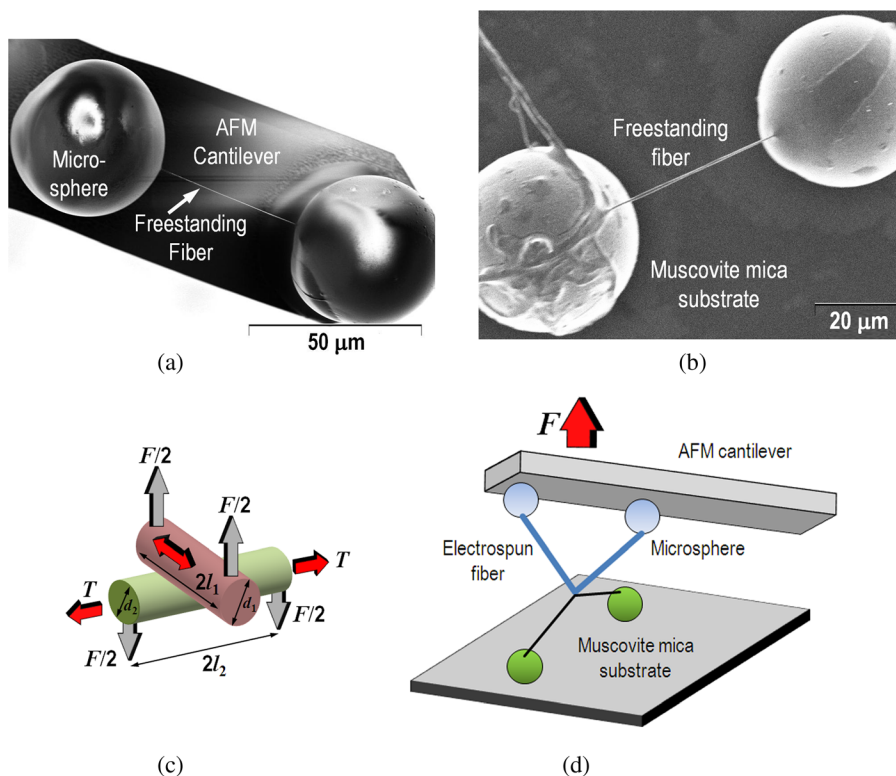


FIG. 1. (Color online) (a) Scanning electron (SEM) micrograph of a nano-cheese-cutter at one end of an AFM cantilever. (b) SEM micrograph of an overhanging freestanding fiber on mica substrate. (c) Schematic of the contact between two fibers arranged in a crossed-cylinder geometry. (d) In the presence of external tension, the cheese-cutter (top) deforms into V-shape and the overhanging fiber (bottom) an inverted V-shape.



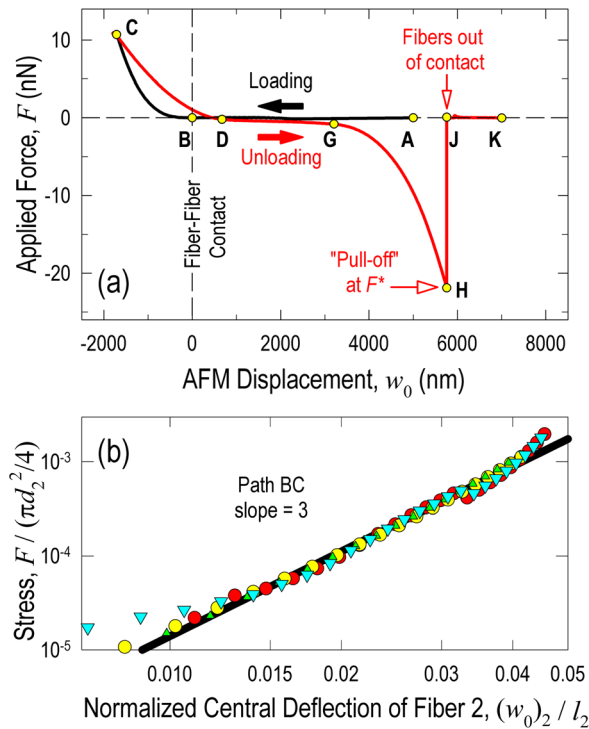


FIG. 2. (Color online) (a) Typical force-displacement measurement showing paths of loading (ABC) and unloading (CDGHJK). Here  $d_1 = 109 \pm 16$  nm and  $l_1 = 91 \pm 4.8$   $\mu$ m, and  $d_2 = 580 \pm 20$  nm and  $l_2 = 97 \pm 5$   $\mu$ m. (b) Force curve along path BC for several sample fibers and curve fit. Only every other fifth data point is shown for clarity.

modulus was found to be  $E = 14.70 \pm 0.75$  GPa. The designated maximum vertical displacement,  $(w_0)_{max}$ , was reached at C. Upon unloading, the cantilever retracted along CD, which did not retrace BC due to fiber viscoelasticity. Plastic deformation was ruled out because subsequent loading-unloading cycles were reversible (see later). Along DG, the external load virtually vanished ( $F \approx 0$ ), indicating either one or both fibers were sagging. At G, the fibers became taut again and the applied load turned tensile ( $F < 0$ ). The fibers deformed along GH into a mirror image to CD, with the cheese-cutter now in a V-shape (Fig. 1(d)). The two force curves of CD and GH coincided if one  $F$  was reversed in sign, and yielded the same elastic modulus. At H, an instability of “pull-off” occurred when the fibers spontaneously detached from each other at a critical tensile “pull-off” force,  $F^*$ . The external load then vanished at J, and no further inter-fiber interaction was observed along JK and beyond. Force measurements were repeated using the same cheese-cutter but several fibers on the mica substrate with ranges of  $d_2$  and  $l_2$  as shown in Fig. 3(a). Without loss of generality, all force curves,  $F(w_0)$ , were artificially shifted to coincide at “pull-off” in order to compare  $F^*$ . The cheese-cutter was believed to be sagging, since all  $F(w_0)$  showed similar characteristics (cf. DG in Fig. 2). The larger the pull-off force, the stronger the adhesion and thus higher the adhesion energy,  $\gamma$ . Appendix B outlines the adhesion model used to extract the materials parameter. Since the Tabor parameter falls in the range of  $\mu_T \approx 0.1$  to 0.15, the Derjaguin-Muller-Toporov (DMT) theory<sup>20</sup> is assumed here which gives  $F^* = -\pi d \gamma$  with the effective diameter,  $d = (d_1^{-1} + d_2^{-1})^{-1}$ . The interfacial adhesion energy is found to be  $\gamma = 71.0 \pm 13.3$

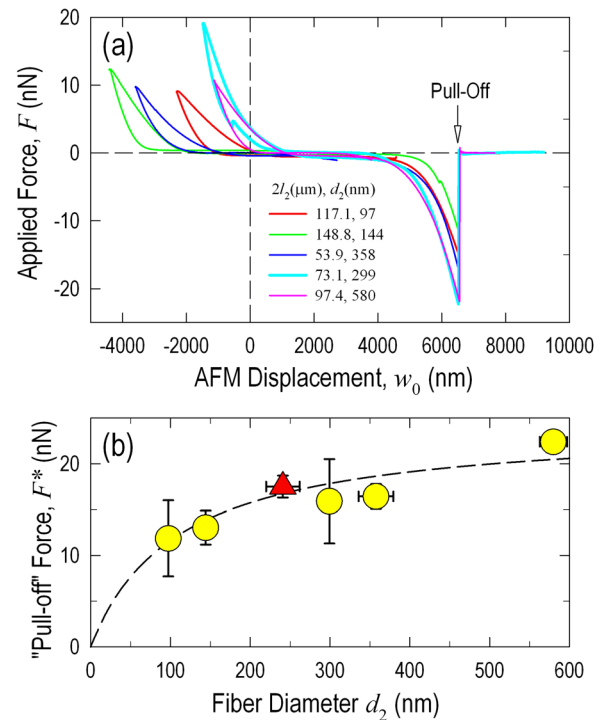


FIG. 3. (Color online) (a) Force measurements of the same fiber on AFM cantilever ( $d_1 = 109 \pm 16$  nm and  $l_1 = 91 \pm 4.8$   $\mu$ m) adhering to fibers on mica with  $d_2$  and  $l_2$  indicated. (b) Pull-off force as a function of mica fiber diameter. Circles are data from first fiber on AFM (cf. Fig. 3(a)) and triangle from second fiber on AFM (cf. Fig. 4(a)). Dashed curve shows the DMT prediction based on  $d_1 = 109 \pm 16$  nm and  $\gamma = 71.0 \pm 13.3$  mJ  $\cdot$  m<sup>-2</sup>.

mJ  $\cdot$  m<sup>-2</sup>. Figure 3(b) shows  $F^*$  as a function of  $d_2$  fitted to the theoretical model. Adhesion is fairly independent of the fiber diameter for Nylon 6, contrasting other fibers that show an increasing adhesion for smaller diameters.<sup>21–23</sup>

To ensure consistency, another nano-cheese-cutter was prepared on yet another AFM cantilever. Figure 4(a) shows the loading-unloading cycles in the same two fibers. Both fibers appeared to be initially taut and throughout loading, because the  $F = 0$  section between unloading and “pull-off” was clearly absent (cf. path DG in Fig. 2). Contrasting the first cheese-cutter, the initial compressive load gave rise to a linear rather than cubic  $F(w_0)$ . Here the maximum central displacement of each fiber was roughly its diameter,  $(w_0)_{max} \sim d$ , fiber bending, rather than stretching, is the dominant deformation mode, and Eq. (A8) reduces to  $F = (3\pi E d^4 / 8 l^3) w_0$ . For two interacting fibers,

$$F = \frac{3\pi E}{8} \left( \frac{l_1^3}{d_1^4} + \frac{l_2^3}{d_2^4} \right)^{-1} w_0. \quad (2)$$

The elastic modulus matches with the value found in the first cheese-cutter. The first five loading-unloading cycles showed virtually identical force measurement  $F(w_0)$ , indicating reversibility of elastic deformation and even adhesion-detachment. The subsequent five cycles showed progressive deviation with increased sagging length and wiggles in  $F(w_0)$ , presumably due to plastic yielding, surface roughening, degradation and wear at the small fiber-fiber contact after multiple detachments. Figure 4(b) shows  $F^*$  as a function of loading-unloading cycles, suggesting a fairly constant

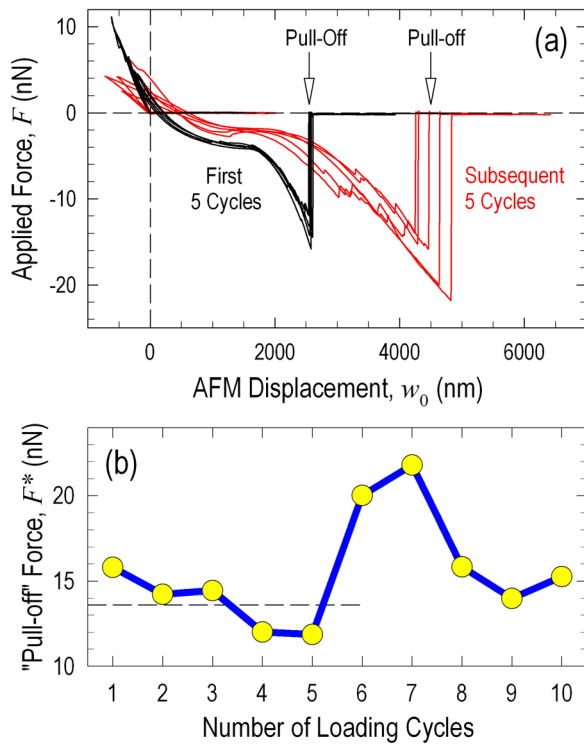


FIG. 4. (Color online) (a) Loading-unloading cycles performed by fibers with  $d_1 = 140 \pm 13$  nm and  $l_1 = 42.73 \pm 0.27$   $\mu\text{m}$ , and  $d_2 = 241 \pm 36$  nm and  $l_2 = 36.66 \pm 0.04$   $\mu\text{m}$ . (b) “Pull-off” force as a function of loading cycles. Adhesion energy deduced from  $F^*$  measured in the first 5 cycles is  $\gamma = 62.9 \pm 10.7$   $\text{mJ} \cdot \text{m}^{-2}$  (dashed line).

adhesion energy at least in the first 5 runs. These measurements were specific to the system described above. The number of reversible loading-unloading cycles and degree of deterioration might vary accordingly, if the dimension, yield strength and materials nature of the fibers, as well as the maximum vertical displacement of the nano-cheese-cutter, were changed.

### III. DISCUSSION

We have demonstrated direct adhesion measurement of two freestanding polymer nano-fibers at right angle using a nano-cheese-cutter. The technique offers a number of unique features: (i) contrasting the point load in conventional AFM probes and nano-indenters, the present geometry allows a line load to be applied to a sample; (ii) both elastic modulus and adhesion strength can be measured in a single setup; (iii) the two interacting fibers can be made similar or dissimilar, e.g., different chemistry, with/without coating, and hollow/solid fibers, etc; and (iii) experiments can be conducted in a desirable aqueous environment at elevated temperature.

Despite the remarkable similarity in the crossed-cylinder geometry, the nano-cheese-cutter is quite different from the surface force apparatus (SFA).<sup>18</sup> In SFA, atomically smooth mica flakes are attached to the surface of two large glass cylinders. Upon a compressive load, an adhesion contact circle is produced where the stress within is governed by the Hertz contact theory. Elastic modulus can be measured but is essentially confined to the compression mode. The adhesion energy is deduced from the measured critical “pull-

off” force. The relatively large contact area usually leads to the Johnson–Kendall–Roberts (JKR) type of adhesion mechanics. In contrary, in a nano-cheese-cutter, radii of the two cylindrical fibers are much smaller. Local deformation at the contact circle is too small to be characterized, but the global stretching of the fiber along its length can be accurately measured and the elastic modulus of tension deduced. The very small contact circle here makes the intersurface force range appear large, and thus the Derjaguin–Muller–Toporov (DMT) type of adhesion is applicable. The nano-cheese-cutter provides a unique way to gauge mechanical integrity of individual fiber and fiber mesh.

### IV. CONCLUSION

A nano-cheese-cutter is designed and fabricated to directly measure the elastic modulus of electrospun nano-fibers and adhesion energy of fiber-fiber interface. The technique is also capable of investigating fatigue and repeated adhesion-detachment. The measurements have significant impact in the mechanical performance of fiber mesh where inter-fiber adhesion holds the key to integrity, as well as performance of micro-/nano-devices with movable bridges and cantilevers.

### ACKNOWLEDGMENTS

This work was supported by the National Science Foundation through Grants CMMI No. 0757140 and CMMI No. 0746703. Any opinions, findings, and conclusions or recommendations expressed in this material are those of the authors and do not necessarily reflect the views of the NSF. We acknowledge Professor Sinan Muftu, Professor Jeffrey Ruberti, and Dr. Sivasubramanian Somu at Northeastern University for their invaluable discussions.

### APPENDIX A: THEORETICAL MODEL FOR CLAMPED FIBER UNDER CENTRAL LOAD

The linear elastic solution for a clamped fiber deformed under mixed bending and stretching is not available in literature. The analytical solution is derived from the first principles for a single fiber deformed at the midpoint. Figure 5 shows a residual stress free fiber with diameter,  $d$ , length,  $2l$ , elastic modulus,  $E$ ,

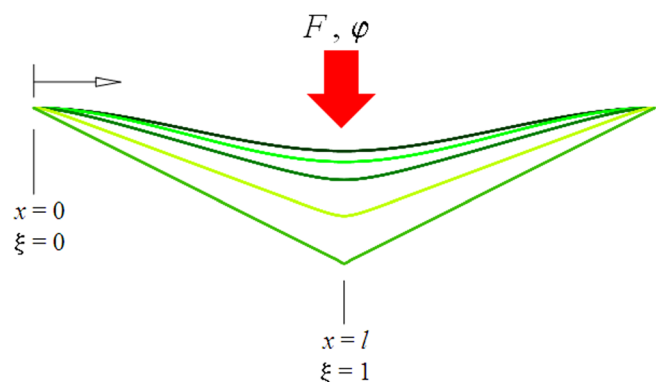


FIG. 5. (Color online) Schematic of a freestanding fiber loaded at the midpoint for several central displacements.

being loaded at the midpoint by an external load,  $F$ . Elastic deformation occurs and the fiber profile becomes  $w(x)$  with  $x$  being the distance from one clamped end and a central displacement,  $w_0 = w(x=l)$ . The governing equation is given by

$$\kappa \nabla^4 w - T \nabla^2 w = F \delta(x) \quad (\text{A1a})$$

with  $\nabla^2$  the Laplacian operator in rectangular coordinates. Equation (A1a) can be rewritten as

$$\kappa \frac{\partial^2 w}{\partial x^2} - Tw = -\left(\frac{F}{2}\right)x - M_0 \quad (\text{A1b})$$

with the bending moment  $M_0 = M|_{x=0}$ . Boundary conditions are identified as  $w(x=0) = 0$  and  $w'(x=0) = w'(x=l) = 0$  with  $' = \partial/\partial x$ . The stress-strain relation is given by  $\sigma = E \varepsilon$ , or

$$\sigma = \frac{T}{\pi d^2/4} = \frac{E}{l} \int_0^l (\sec \theta - 1) dx \approx \frac{E}{l} \int_0^l \frac{1}{2} \left(\frac{dw}{dx}\right)^2 dx \quad (\text{A2})$$

for  $\theta = \partial w/\partial x$  and  $\sec \theta \approx 1 + \theta^2/2$  for small  $\theta$ . For simplicity, a set of dimensionless parameters are defined as follows:

$$\xi = \frac{x}{l}, \quad \omega = \frac{w}{d}, \quad \beta = \sqrt{\frac{l^2 T}{\kappa}}, \quad \varphi = \frac{F l^3}{2 \kappa d}, \quad m_0 = \frac{M_0 l^2}{\kappa d}.$$

Therefore, Eqs. (A1b) and (A2) become

$$\omega'' - \beta^2 \omega = -\varphi \xi - m_0, \quad (\text{A3})$$

$$\beta^2 = \int_0^1 \left(\frac{d\omega}{d\xi}\right)^2 d\xi, \quad (\text{A4})$$

respectively, with  $\omega(\xi=0) = 0$  and  $\omega'(\xi=0) = \omega'(\xi=1) = 0$  with  $' = \partial/\partial \xi$ . An analytical solution to Eq. (A3) is found to be

$$\omega = \frac{\varphi}{\beta^3} \left\{ -\sinh(\beta \xi) + \left[ \frac{\cosh \beta - 1}{\sinh \beta} \right] [\cosh(\beta \xi) - 1] + \beta \xi \right\} \quad (\text{A5})$$

with a central deflection  $\omega_0 = \omega(\xi=1)$  becomes

$$\omega_0 = \sqrt{\frac{\beta^7 (1 + e^\beta)^2}{16 e^\beta (2\beta + \beta \cosh \beta - 3 \sinh \beta)}} \left[ \frac{2 + \beta + e^\beta (\beta - 2)}{\beta^3 (1 + e^\beta)} \right]. \quad (\text{A6})$$

Substituting (A5) into (A4) yields

$$\varphi = \sqrt{\frac{\beta^7 (1 + e^\beta)^2}{16 e^\beta (2\beta + \beta \cosh \beta - 3 \sinh \beta)}}. \quad (\text{A7})$$

The exact constitutive relation,  $\varphi(\omega_0)$ , can be found by treating  $\beta$  as a varying parameter as both  $\varphi(\beta)$  and  $\omega_0(\beta)$  are functions of  $\beta$ . It can be shown that  $\varphi \propto (\omega_0)^n$ , where  $n$  is the gradient given by  $n = \partial(\log \varphi)/\partial(\log \omega_0)$ . The exact expressions for  $n(\omega_0)$  or  $n(\varphi)$  can be obtained by software such as MATHEMATICA but are too lengthy to be explicitly stated here.

Thick and stiff fibers possess a large  $\kappa$  with minimal axial stretching. Therefore,  $\beta \rightarrow 0$  and bending is dominant. In such limit, equations (A5)–(A7) reduce to

$$\omega = \frac{\varphi}{2} \left( \frac{\xi^2}{2} - \frac{\xi^3}{3} \right) \text{ and } \varphi = 12 \omega_0 \quad (\text{A8})$$

or,  $\varphi \propto \omega_0$ , with  $n = 1$ . The deformed profile and linear constitutive relation match with the classical elastic solution.<sup>1,2</sup> On the other hand, thin and flexible fibers possess minimal  $\kappa$ ,  $\beta \rightarrow \infty$  and stretching dominates. In the limit

$$\omega = \omega_0 \xi \text{ and } \varphi = 8 \omega_0^3 \quad (\text{A9})$$

or,  $\varphi \propto (\omega_0)^3$ , with  $n = 3$ . The fiber is a classic V-shape with straight overhanging arms. Such solution is not available in classical linear elasticity literature. Note that equations (A8)–(A9) are equivalent to equations (A5)–(A7). Behavior of fibers with intermediate diameter and stiffness and an intermediate  $\beta$  thus lie between the two limits. The bending-stretching transition occurs at roughly  $\omega_0 \sim 1$  or  $w_0 \sim d$ . Figure 6(a) shows the changing deformed profile as the applied load increases with  $\beta$ . A V-shape is expected in the stretching limit. Note that  $w(r)$  is a smooth curve with zero gradients at clamped ends and midpoint when load is small, but becomes a V-shape with straight arms at large loads.

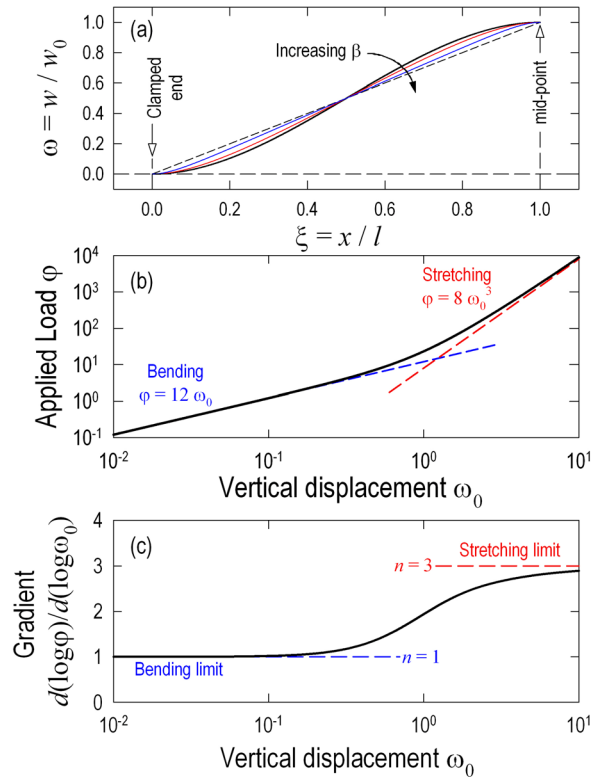


FIG. 6. (Color online) (a) Normalized deformed profiles for fiber tension  $\beta = 0, 7, 20$ , and the stretching limit  $\beta \rightarrow \infty$  (dashed curve). Note that the slope at  $x=0$  is always zero, but approaches a constant only in the limit when the profile becomes linear. (b) The constitutive relation  $\varphi(\omega_0)$ , and the bending and stretching limits (dashed lines). Bending dominates at small  $\omega_0$ , while stretching prevails at large  $\omega_0$ . (c) Gradient of the constitutive relation as a function of vertical displacement,  $n(\omega_0)$ .

Figure 6(b) shows the constitutive relation,  $\varphi(\omega_0)$ . Initial loading is always governed by bending when  $\omega_0 < 1$ . As external load increases, deformation gradually switches to stretching dominant. Figure 6(c) shows the gradient of  $\varphi(\omega_0)$  as a function of vertical displacement and the bending and stretching limits of 1 and 3, respectively.

## APPENDIX B: “PULL-OFF” FORCE AND ADHESION ENERGY OF ADHERING FIBERS

“Pull-off” or spontaneous detachment of the two adhering fibers is similar to that of the surface force apparatus.<sup>18</sup> The critical phenomenon is approximated by adhesion of a solid sphere with diameter,  $d$ , and interfacial adhesion energy,  $\gamma$ , onto a rigid substrate. Maugis<sup>20</sup> shows that the tensile load required for “pull-off” is given by

$$F^* = -\phi\pi(d/2)\gamma, \quad (\text{B1})$$

where  $d = (d_1^{-1} + d_2^{-1})^{-1}$  is effective fiber diameter. The parameter  $\phi$  is bounded by  $3/2 < \phi < 2$ , where the upper bound ( $\phi = 2$ ) is the Derjaguin–Muller–Toporov (DMT) limit for small but hard spheres in the presence of weak but long-range intersurface attraction, and the lower bound ( $\phi = 3/2$ ) is the Johnson–Kendall–Roberts (JKR) limit for large but soft spheres in the presence of strong but short-range adhesion. The intermediate behavior between the JKR to DMT limits is governed by the Tabor’s parameter

$$\mu_T = \left(\frac{\gamma^2 R}{Z_0^3}\right)^{1/3} \left[\frac{E}{2(1-\nu^2)}\right]^{-2/3} \quad (\text{B2})$$

with  $Z_0 \approx 1$  nm the force range of typical van der Waals interactions,  $E$  and  $\nu$  the elastic modulus and Poisson’s ratio of the spheres. Large  $\mu_T > 2$  corresponds to JKR and small  $\mu_T < 0.5$  DMT. For the interacting fibers in the present

study,  $\mu_T \approx 0.1$  to 0.15 and DMT limit is assumed in data analysis.

- <sup>1</sup>G. Duan and K.-T. Wan, *Int. J. Mech. Sci.* **52**, 1158 (2010).
- <sup>2</sup>B. Bhushan, *J. Vac. Sci. Technol. B* **21**, 2262 (2003).
- <sup>3</sup>Y. Dzenis, *Science* **304**, 1917 (2004).
- <sup>4</sup>D. H. Reneker, A. L. Yarin, E. Zussman, and H. Xu, *Adv. Appl. Mech.* **41**, 43 (2007).
- <sup>5</sup>S. Sundararajan and S. Ramakrishna, *J. Mater. Sci.* **42**, 8400 (2007).
- <sup>6</sup>C. Meechaisue, P. Wutticharoenmongkol, R. Waraput, T. Huangjing, N. Ketbumrung, P. Pavasant, and P. Supaphol, *Biomed. Mater.* **2**, 181 (2007).
- <sup>7</sup>C. T. Gibson, D. J. Johnson, C. Anderson, C. Abell, and T. Rayment, *Rev. Sci. Instrum.* **75**, 565 (2004).
- <sup>8</sup>Z. Jing, X. Y. Xu, X. S. Chen, Q. Z. Liang, X. C. Bian, L. X. Yang, and X. B. Jing, *J. Control. Release* **92**, 227 (2003).
- <sup>9</sup>Z. Zong, C.-L. Chen, M. R. Dokmeci, and K.-T. Wan, *J. Appl. Phys.* **107**, 026104 (2010).
- <sup>10</sup>Q. Shi, K.-T. Wan, S. C. Wong, P. Chen, and T. A. Blackledge, *Langmuir* **26**, 14188 (2010).
- <sup>11</sup>J. D. Whittaker, E. D. Minot, D. M. Tanenbaum, P. L. McEuen, and R. C. Davis, *Nano Lett.* **6**, 953 (2006).
- <sup>12</sup>T. Tang, A. Jogota, and C.-Y. Hui, *J. Appl. Phys.* **97**, 074304 (2005).
- <sup>13</sup>S. Vajpayee, A. Jagota, and C.-Y. Hui, *J. Adhesion* **86**, 39 (2010).
- <sup>14</sup>S. Manohar, A. Mantz, K. Bancroft, C.-Y. Hui, A. Jagota, and D. Vezenov, *Nano Lett.* **8**, 4365 (2008).
- <sup>15</sup>R. Chen, C. Huang, Q. F. Ke, C. L. He, H. S. Wang, and X. M. Mo, *Colloid. Surf. B* **79**, 315 (2010).
- <sup>16</sup>P. Peng, Y. Z. Chen, Y. F. Gao, J. Yu, and Z. X. Guo, *J. Polym. Sci., Part B* **47**, 1853 (2009).
- <sup>17</sup>D. Almecija, D. Blond, J. E. Sader, J. N. Coleman, and J. J. Boland, *Carbon* **47**, 2253 (2009).
- <sup>18</sup>J. N. Israelachvili, *Intermolecular and Surface Forces*, 3rd ed. (Academic Press, London, 2011).
- <sup>19</sup>J. P. Cleveland, S. Manne, D. Bocek, and P. K. Hansma, *Rev. Sci. Instrum.* **64**, 403 (1993).
- <sup>20</sup>D. Maugis, *Contact, Adhesion and Rupture of Elastic Solids* (Springer, New York, 2000).
- <sup>21</sup>A. Arinstein, M. Burman, O. Gendelman, and E. Zussman, *Nat. Nanotech.* **2**, 59 (2007).
- <sup>22</sup>P. J. I. T. Veld, M. Hütter, and G. C. Rutledge, *Macromol.* **39**, 439 (2006).
- <sup>23</sup>S. C. Wong, A. Baji, and S. Leng, *Polymer* **49**, 4713 (2008).